Autophagy 11:9, 1471–1483; September 2015; © 2015 Taylor & Francis Group, LLC

Expression of a ULK1/2 binding-deficient ATG13 variant can partially restore autophagic activity in ATG13-deficient cells

Nora Hieke,[1,†] Antje S Löffler,[1,†] Takeshi Kaizuka,[2,3,†] Niklas Berleth,[1] Philip Böhler,[1] Stefan Drießen,[1] Fabian Stuhldreier,[1] Olena Friesen,[1] Kaivon Assani,[4] Katharina Schmitz,[1] Christoph Peter,[1] Britta Diedrich,[5] Jörn Dengjel,[5] Petter Holland,[6] Anne Simonsen,[6] Sebastian Wesselborg,[1] Noboru Mizushima,[2,3] and Björn Stork[1,*]

[1]Institute of Molecular Medicine I; Heinrich-Heine-University; Düsseldorf, Germany; [2]Department of Biochemistry and Molecular Biology; Graduate School and Faculty of Medicine; University of Tokyo; Tokyo, Japan; [3]Department of Physiology and cell Biology; Tokyo Medical and Dental University; Tokyo, Japan; [4]Center for Microbial Pathogenesis; The Research Institute at Nationwide Children's Hospital; Columbus, OH USA; [5]Department of Dermatology; Medical Center; ZBSA Center for Biological Systems Analysis; BIOSS Centre for Biological Signaling Studies; Freiburg Institute for Advanced Studies; University of Freiburg; Freiburg, Germany; [6]Institute of Basic Medical Sciences; Faculty of Medicine; University of Oslo; Oslo, Norway

[†]These authors contributed equally to this work.

Keywords: ATG13, ATG101, autophagy, RB1CC1, ULK1

Abbreviations: ACTB/β-actin, actin, β; AMPK, AMP-activated protein kinase; ATG, autophagy-related; Baf A1, bafilomycin A_1; BECN1, Beclin 1, autophagy-related; EBSS, Earle's balanced salt solution; GFP, green fluorescent protein; GST, glutathione S-transferase; KO, knockout; LIR, LC3-interacting region; MAP1LC3/LC3, microtubule-associated protein 1 light chain 3; MEF, mouse embryonic fibroblast; MIM, MIT-interacting motif; MIT, microtubule interacting and transport; (M)TOR, (mechanistic) target of rapamycin (serine/threonine kinase); PAS, phagophore assembly site; PtdIns3K, phosphatidylinositol 3-kinase; RB1CC1/FIP200, RB1-inducible coiled-coil 1; SQSTM1/p62, sequestosome 1; ULK1/2, unc-51 like autophagy activating kinase 1/2.

Autophagy describes an intracellular process responsible for the lysosome-dependent degradation of cytosolic components. The ULK1/2 complex comprising the kinase ULK1/2 and the accessory proteins ATG13, RB1CC1, and ATG101 has been identified as a central player in the autophagy network, and it represents the main entry point for autophagy-regulating kinases such as MTOR and AMPK. It is generally accepted that the ULK1 complex is constitutively assembled independent of nutrient supply. Here we report the characterization of the ATG13 region required for the binding of ULK1/2. This binding site is established by an extremely short peptide motif at the C terminus of ATG13. This motif is mandatory for the recruitment of ULK1 into the autophagy-initiating high-molecular mass complex. Expression of a ULK1/2 binding-deficient ATG13 variant in ATG13-deficient cells resulted in diminished but not completely abolished autophagic activity. Collectively, we propose that autophagy can be executed by mechanisms that are dependent or independent of the ULK1/2-ATG13 interaction.

Introduction

Macroautophagy (hereafter referred to as autophagy) describes a process for the degradation of cytoplasmic contents including long-lived, misfolded or aggregated proteins, or entire organelles. In yeast and higher eukaryotic cells this mechanism is evolutionarily conserved and represents a major player in the degradation network next to the ubiquitin-proteasome-system. Under regular physiologic conditions, basal autophagy executes a critical role in cell homeostasis through protein and organelle quality control. However, autophagy can be upregulated under stress conditions like ATP or amino acid deprivation, hypoxia, growth factor withdrawal, DNA damage, or intracellular pathogens. During autophagy, phagophores form at phosphatidylinositol-3-phosphate (PtdIns3P)-enriched microdomains in the endoplasmic reticulum (ER) termed omegasomes, and the expanding phagophores engulf portions of cytoplasmic material. Closure of this membrane compartment gives rise to autophagosomes. Autophagosomes are double-membraned vesicles which then fuse with endosomes and lysosomes resulting in the formation of autolysosomes.[1] Lysosomal hydrolases subsequently degrade the cargo as well as the inner vesicular membrane, and the resulting building blocks such as amino or fatty acids are made available for *de novo* protein synthesis, ATP generation, and so forth.

On the molecular level, autophagy-related (ATG) gene products as well as several non-ATG proteins regulate all steps

*Correspondence to: Björn Stork; Email: bjoern.stork@uni-duesseldorf.de
Submitted: 09/02/2014; Revised: 06/22/2015; Accepted: 06/27/2015
http://dx.doi.org/10.1080/15548627.2015.1068488

of the autophagic flux, including vesicle nucleation, elongation, closure, and fusion with endosomes and lysosomes.[2] With regard to autophagy initiation, the ULK1/2 kinase complex has been characterized as central gatekeeper. In 2009, several groups clarified the composition of this complex and its molecular regulation by the upstream nutrient-sensing MTORC1.[3-8] The macromolecular ULK1/2 (unc51-like autophagy activating kinase 1/2) complex with a molecular mass of approximately 3 MDa is comprised of the Ser/Thr protein kinase ULK1/2 and the accessory proteins ATG13, RB1CC1/FIP200 (RB1-inducible coiled-coil 1), and ATG101.[3-5] In the currently accepted model, the components of the ULK1/2 complex are constitutively associated irrespectively of nutrient supply. Under nutrient-rich conditions, MTORC1 interacts with the ULK1/2 complex, resulting in the inactivation of the complex by MTOR-dependent phosphorylation of ULK1/2 and ATG13 and thus in the inhibition of autophagy. During nutrient deprivation, MTORC1 dissociates from the complex, leading to the activation of the complex by ULK1/2-dependent autophosphorylation and transphosphorylation of ATG13 and RB1CC1 and thus to autophagy induction. However, it appears that the above-described model represents a rather simplistic view. For example, the MTOR-dependent phospho-sites of ATG13 or the ULK1/2-dependent phospho-sites of RB1CC1 have not been reported so far, and the importance of ULK1/2-dependent phosphorylation of ATG13 has been questioned.[9] Furthermore, it has been recently shown that ULK1 is directly controlled by other kinases, e.g. the energy-sensing AMP-activated protein kinase (AMPK) or AKT,[10-14] and by alternative post-translational modifications, e.g. acetylation or ubiquitination.[15,16] With regard to ULK1 ubiquitination, it appears that this is another mode of action for how MTOR influences ULK1 activity. It has been reported that MTORC1 phosphorylates AMBRA1 and thus inhibits TRAF6-mediated ubiquitination of ULK1, which is required for stabilization and activation.[16] Downstream of ULK1, several substrates have been identified to mediate the proautophagic function of this kinase, including AMBRA1, BECN1, or DAPK3/ZIPK (death-associated protein kinase 3).[17-19] Of note, ULK1-independent mechanisms of autophagy induction have been proposed as well.[9,20] In contrast, both ATG13 and RB1CC1 appear to be unequivocally required for starvation-induced autophagy.[3,4,6-9,21,22]

In this study, we further elucidated the molecular details of how the ULK1/2 kinase complex regulates autophagy. We observed that the interaction of ATG13 and ULK1/2 requires the last 2 amino acids LQ of ATG13. Deletion of this short peptide motif constitutes an ULK1/2 binding-deficient ATG13 variant, which retains regular binding to RB1CC1 and ATG101. Accordingly, the disruption of the ULK1/2-ATG13 interaction excludes ULK1 but not ATG13 from the autophagy-initiating high-molecular mass complex and abolishes recruitment of ULK1 to the phagophore assembly site (PAS). Interestingly, we observed that autophagy is not completely inhibited in cells expressing the ULK1/2 binding-deficient variant of ATG13. We hypothesize that the interaction of ATG13 and ULK1/2 is not necessarily required for autophagy induction by amino acid deprivation and that ULK1/2-ATG13 interaction-dependent and -independent mechanisms contribute to autophagy.

Results

The interaction between ULK1/2 and ATG13 is controlled by the extreme C terminus of ATG13

The binding site of ULK1 within ATG13 has been roughly mapped to the last 57 amino acids of the C terminus of ATG13.[7] In order to characterize the binding motif essential for the interaction with ULK1/2, we made use of different truncated ATG13 variants, lacking the last amino acid Gln 480/Q480 (1AAΔ), the last 2 amino acids Leu,Gln480/LQ480 (2AAΔ), or the last 3 amino acids Thr,Leu,Gln480/TLQ480 (3AAΔ, amino acid numbering of human isoform 2, Uniprot identifier O75143-2). The latter sequence has previously gained our interest since it contains a putative ULK1 phosphorylation site (Thr478).[9] We also included the 57AAΔ variant as positive control and an F429A and F433A (F429A,F433A) double mutant of ATG13, since it has been previously suggested that these 2 phenylalanine residues might be orthologous to hydrophobic residues of the MIT-interacting motif (MIM) domain in yeast Atg13 mediating the interaction with yeast Atg1.[23] We transiently coexpressed GST fusion proteins of full-length ATG13 or the different ATG13 variants in Flp-In™ T-REx™ 293 cells expressing GFP-tagged full-length ULK1 (GFP-ULK1) or full-length ULK2 (GFP-ULK2), and performed affinity purifications using glutathione-sepharose 4B beads. Only GST-ATG13, GST-ATG13$^{1AA\Delta}$ and GST-ATG13^{F429A,F433A} purified GFP-ULK1 and GFP-ULK2 from Flp-In™ T-REx™ 293 cells in considerable amounts, whereas GST-ATG13$^{2AA\Delta}$ and GST-ATG13$^{3AA\Delta}$ only purified minute amounts of GFP-ULK1 or GFP-ULK2, similar to the 57AAΔ variant (**Fig. 1A**, middle panels). All GST-ATG13 variants purified similar amounts of RB1CC1, except for the 57AAΔ variant which revealed slightly reduced binding to RB1CC1 (**Fig. 1A**, middle panels). In a vice versa approach, the GFP-tagged ULK proteins were immunopurified using GFP-Trap® beads. Again, only GST-ATG13 and GST-ATG13$^{1AA\Delta}$ revealed strong interaction with GFP-ULK1 and GFP-ULK2, whereas only low amounts of GST-ATG13$^{2AA\Delta}$, GST-ATG13$^{3AA\Delta}$, and GST-ATG13$^{57AA\Delta}$ were purified with these 2 proteins (**Fig. 1A**, right panels). GST-ATG13^{F429A,F433A} was clearly purified with GFP-ULK1 but to a lesser extent with GFP-ULK2. In the next step, we investigated whether starvation has an effect on the binding of GFP-ULK1 to the different ATG13 variants. For that, we repeated affinity and immunopurification experiments described above with GST fusion proteins of wild-type ATG13 and ATG13$^{3AA\Delta}$. As a control, we included a C-terminally truncated version of ULK1 which does not interact with ATG13. Again the ATG13$^{3AA\Delta}$ variant did not purify GFP-ULK1 and was itself only slightly purified by GFP-ULK1, independent of nutrient supply

(**Fig. 1B**, middle and right panels). The weak purification of GFP-ULK proteins with 2AAΔ, 3AAΔ and 57AAΔ mutant proteins, and the weak association of these ATG13 variants with GFP-ULKs are probably caused by the heterodimerization of overexpressed GST-ATG13 variants with endogenous ATG13 since ATG13 has been suggested to form dimers.[3] Indeed, endogenous ATG13 can be detected in GFP-ULK1 immunopurifications (**Fig. 1B**, right panels). Similarly, RB1CC1 was purified with GFP-ULK1/2 (**Fig. 1A and B**, right panels), further supporting the presence of endogenous ATG13 (although we could not exclude a direct interaction between ULK1/2 and RB1CC1 at this stage, see below). In order to avoid potential heterodimerization of endogenous ATG13 with overexpressed GST-ATG13 variants, we employed GFP-ULK1-expressing *atg13*$^{-/-}$ (*Atg13* knockout [KO]) murine embryonic fibroblasts (MEFs),[14] that were reconstituted with either HA-tagged full-length ATG13 or the corresponding 3AAΔ deletion mutant. In accordance with our observations previously described, GFP-ULK1 associated with full-length ATG13, but not with ATG13^{3AAΔ} (**Fig. 1C**). Finally, we reconstituted the *Atg13* KO MEFs with different ATG13 variants and analyzed their interaction with endogenous ULK1. Again only wild-type ATG13, ATG13^{1AAΔ} and ATG13^{F429A,F433A} associated with endogenous ULK1, and again this interaction was not affected by nutrient supply. In contrast, ATG13^{2AAΔ}, ATG13^{3AAΔ}, and ATG13^{57AAΔ} did not interact with ULK1. The abolished interaction between ULK1 and ATG13^{3AAΔ} was also confirmed by a mass spectrometry-based SILAC approach (**Fig. S1**). Since the ATG13^{2AAΔ} and the ATG13^{3AAΔ} variants retained normal RB1CC1 binding but no ULK1 binding, it is unlikely that the direct association of ULK1 with RB1CC1 plays a prominent role during the assembly of the heterotetrameric complex. This was also confirmed by the observation that ULK1 was not coimmunopurified with RB1CC1 from lysates derived from *Atg13* KO MEFs (**Fig. S2A**). Similarly, a direct interaction between ATG101 and ULK1 was not detectable in *Atg13* KO MEFs (**Fig. S2B**). Collectively, these data indicate that the interaction between ULK1/2 and ATG13 is mainly controlled by the last 2 amino acids LQ480 of ATG13. Although the ATG13 amino acid sequence shows only weak conservation among species (**Fig. S3A**), the C-terminal TLQ motif is extremely conserved in vertebrates (**Fig. S3B**).

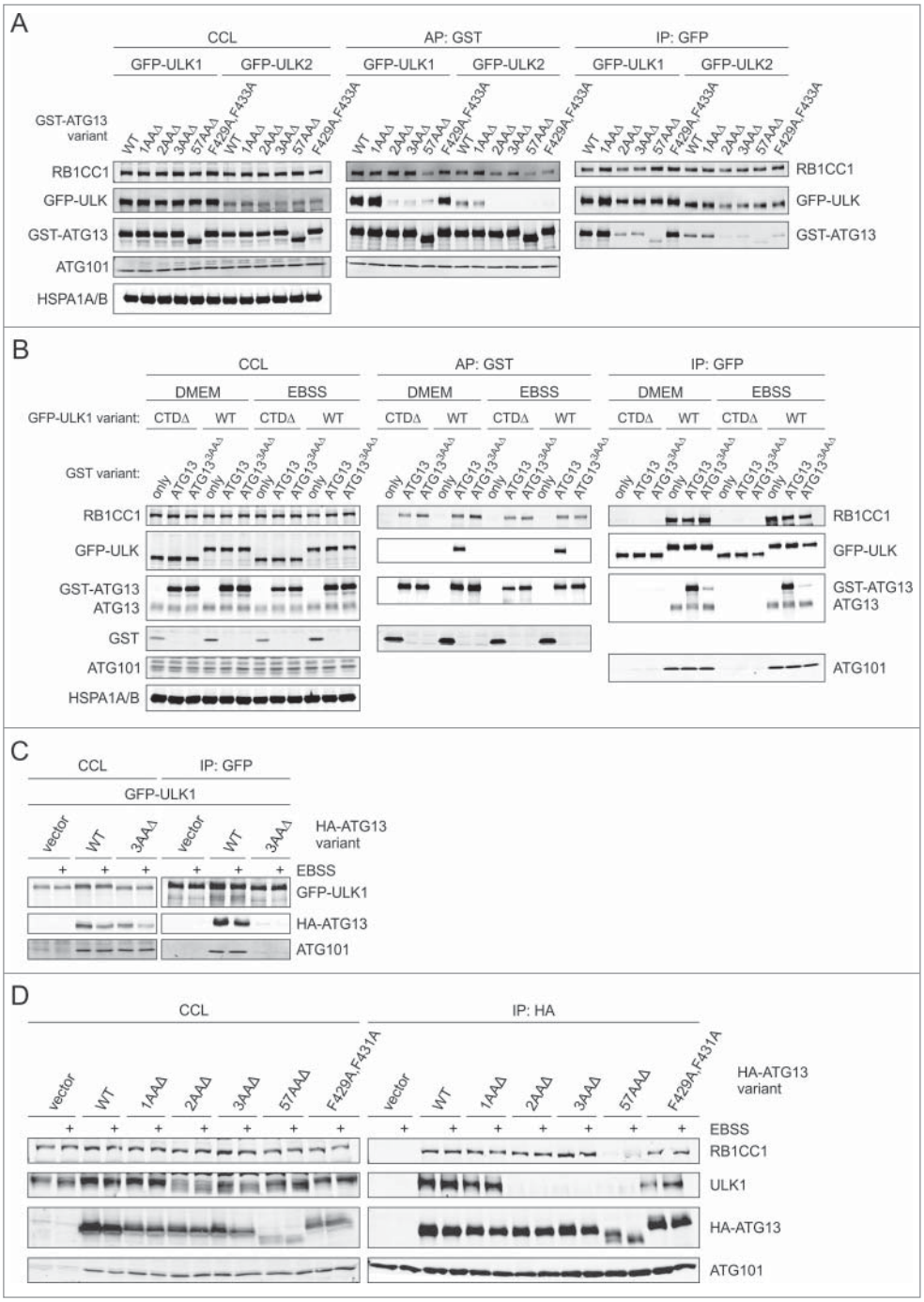

Figure 1. For figure legend, see page 1474.

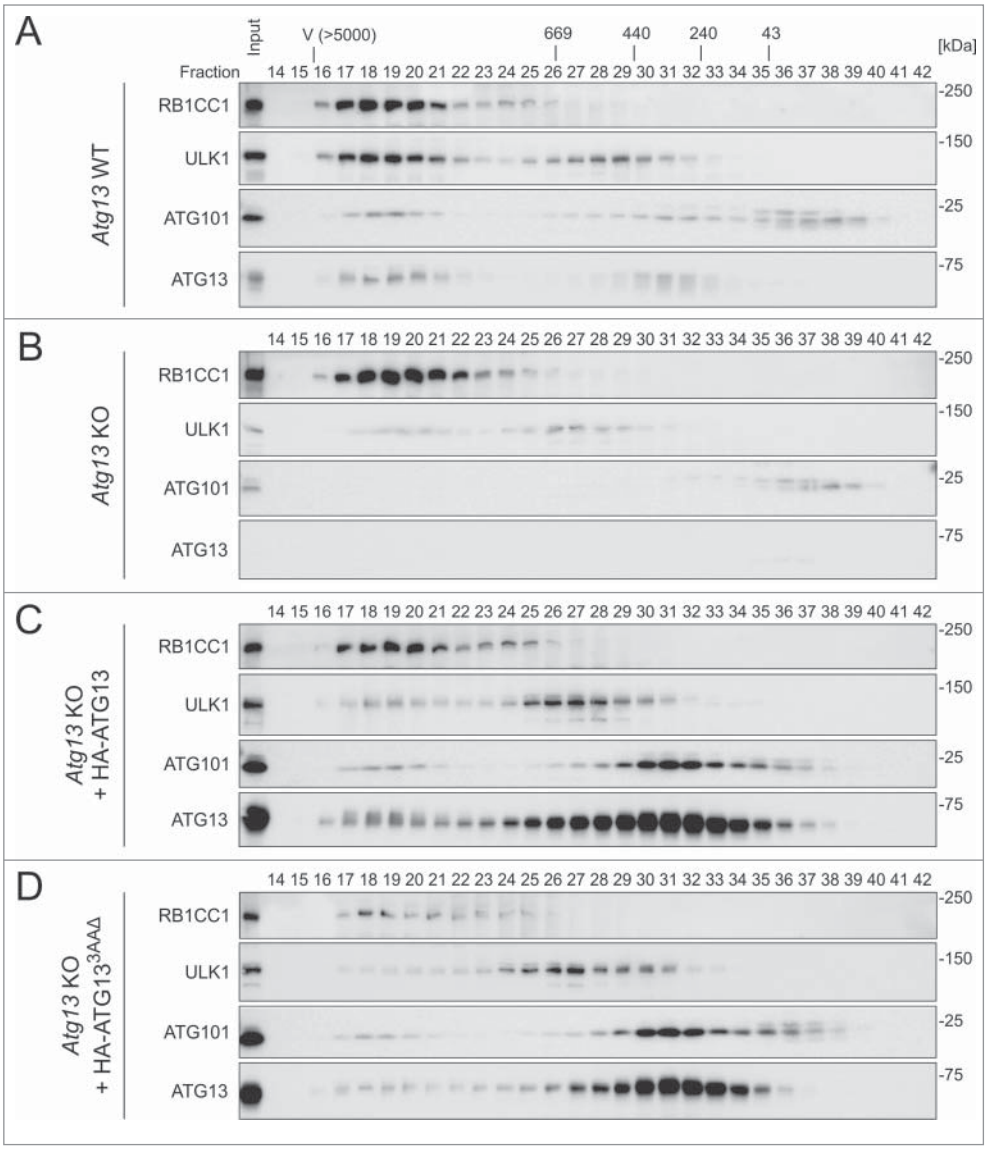

Figure 2. The TLQ480 motif of ATG13 is required for recruitment of ULK1 to the autophagy-regulating complex and the phagophore assembly site. (**A to D**) S100 fractions of wild-type, *Atg13* KO or *Atg13* KO MEFs reconstituted with either HA-ATG13 or HA-ATG13$^{3AA\Delta}$ were separated by size exclusion chromatography on a Superose 6 column. Each fraction was analyzed by immunoblotting with anti-RB1CC1, anti-ULK1, anti-ATG101 and anti-ATG13 antibodies. Positions of the molecular mass standards (in kDa) are shown at the top. V, void fraction.

complex in cells expressing the ULK1/2 binding-deficient ATG13$^{3AA\Delta}$ variant. We deliberately chose the 3AAΔ variant for this and the following experiments, since it apparently cannot bind ULK proteins similar to the 2AAΔ variant, but additionally lacks the putative phospho-acceptor Thr478. To analyze ULK1 recruitment, S100 fractions of wild-type, *Atg13* KO, and *Atg13* KO MEFs reconstituted with either full-length HA-ATG13 or HA-ATG13$^{3AA\Delta}$ were subjected to size exclusion chromatography. For wild-type MEFs, RB1CC1, ULK1, ATG13, and ATG101 were mainly detected in fractions corresponding to a molecular mass of ~3 MDa (**Fig. 2A**) as previously reported.[3-5] ULK1, ATG13 and ATG101 were also eluted in fractions according to lower molecular mass complexes of ~300 to 600 kDa (ULK1), 200 to 400 kDa (ATG13 and ATG101), and <40 kDa (ATG101), confirming previous observations.[4,5] In the absence of ATG13,

The incorporation of ULK1 into the autophagy-initiating complex is mediated by a short peptide motif of ATG13

Next, we were interested whether ULK1 is still recruited to the previously described macromolecular autophagy-initiating

Figure 1 (See previous page). The last 2 amino acids (LQ480) of ATG13 mediate interaction with ULK1/2. (**A**) Flp-In™ T-REx™ 293 cells inducibly expressing GFP-tagged full-length ULK1 (GFP-ULK1) or full-length ULK2 (GFP-ULK2) were transiently transfected with vectors encoding GST-ATG13 (WT), GST-ATG13$^{1AA\Delta}$ (1AAΔ), GST-ATG13$^{2AA\Delta}$ (2AAΔ), GST-ATG13$^{3AA\Delta}$ (3AAΔ), GST-ATG13$^{57AA\Delta}$ (57AAΔ) or GST-ATG13^{F429A,F433A} 12 h before expression of GFP-ULK variants was induced by doxycycline. After 6 h of GFP-ULK induction, cells were lysed and GST affinity purifications (middle panels) or GFP immunopurifications (right panels) were performed. Cleared cellular lysates (CCL) and purified proteins were subjected to SDS-PAGE and analyzed by immunoblotting for RB1CC1, GFP, GST, ATG101, or HSPA1A/B. (**B**) Flp-In™ T-REx™ 293 cells inducibly expressing GFP-tagged ULK1 lacking the C-terminal domain (CTDΔ) or full-length ULK1 (WT) were transiently transfected with vectors encoding GST (only), GST-ATG13 (ATG13) or GST-ATG13$^{3AA\Delta}$ (ATG13$^{3AA\Delta}$) 12 h before expression of GFP-ULK variants was induced by doxycycline. After 4 h of GFP-ULK induction, cells were cultured in regular medium or starvation medium (EBSS) for 2 h. Cells were lysed and GST affinity purifications (middle panels) or GFP immunopurifications (right panels) were performed. Cleared cellular lysates (CCL) and purified proteins were subjected to SDS-PAGE and analyzed by immunoblotting for RB1CC1, GFP, ATG13, GST, ATG101, or HSPA1A/B. (**C**) GFP-ULK1-expressing *Atg13* KO MEFs retrovirally transfected with empty vector or cDNA encoding HA-ATG13 (WT) or HA-ATG13$^{3AA\Delta}$ (3AAΔ) were cultured in regular medium or starvation medium (EBSS) for 2 h. Cells were lysed and GFP-immunopurifications were performed. CCLs and purified proteins were subjected to SDS-PAGE and analyzed by immunoblotting for ULK1, ATG13, or ATG101. (**D**) *Atg13* KO MEFs retrovirally transfected with empty vector or cDNA encoding HA-ATG13 (WT), HA-ATG13$^{1AA\Delta}$ (1AAΔ), HA-ATG13$^{2AA\Delta}$ (2AAΔ), HA-ATG13$^{3AA\Delta}$ (3AAΔ), HA-ATG13$^{57AA\Delta}$ (57AAΔ) or HA-ATG13^{F429A,F433A} were cultured in regular medium or starvation medium (EBSS) for 2 h. Cells were lysed and HA-immunopurifications were performed. CCLs and purified proteins were subjected to SDS-PAGE and analyzed by immunoblotting for RB1CC1, ULK1, ATG13, or ATG101.

ULK1 and ATG101 overall levels are decreased and predominantly present in low molecular fractions, i.e. ~300 to 600 kDa for ULK1 and <40 kDa for ATG101 (**Fig. 2B**). This indicates that ATG13 is essential for the recruitment of ULK1 and ATG101 to the high molecular mass complex established by RB1CC1. Again confirming previous results, the distribution of RB1CC1 is not affected by the absence of ATG13.[4,5] The size exclusion chromatography pattern of *Atg13* KO MEFs reconstituted with HA-tagged full-length ATG13 generally resembles the one observed for wild-type MEFs (**Fig. 2C**). Furthermore, the overall protein levels of ULK1 and ATG101 are normalized or even increased compared to the levels in wild-type or *Atg13* KO MEFs, which is probably caused by the stabilizing effects of ATG13.[3-5,7] Since ATG13 protein levels are higher in this reconstituted cell line than in wild-type MEFs, the main portion of ATG13—and thus the main portions of ULK1 and ATG101—are present in fractions corresponding to 200 to 500 kDa, and only small amounts are incorporated in the high molecular mass complex. Nevertheless, all 3 proteins and RB1CC1 are present in fractions corresponding to the ~3 MDa complex. For the *Atg13* KO MEFs reconstituted with HA-ATG13$^{3AA\Delta}$, only ATG101 was shifted to fractions corresponding to the ~3 MDa complex, while ULK1 largely remained in fractions comprising lower molecular mass complexes of ~300 to 600 kDa (**Fig. 2D**). To confirm the importance of the TLQ-motif for ULK1 recruitment by an independent approach, we transfected the cells described above with cDNA encoding GFP-ULK1 and analyzed starvation-induced formation of GFP-ULK1 puncta. The number of GFP-ULK1 puncta per cell was significantly reduced in cells either lacking ATG13 or expressing the ULK1 binding-deficient variants 3AAΔ or 57AAΔ (**Fig. 3**). Furthermore, colocalization of GFP-ULK1 and HA-ATG13 was only observed for wild-type ATG13 and almost completely absent in the 3AAΔ or 57AAΔ versions. Collectively, these results indicate that the interaction of ATG13 with ULK1 and the recruitment of ULK1 to the autophagy-initiating complex are dependent on the last 3 amino acids of ATG13. Deletion of this TLQ480 motif is sufficient to exclude ULK1 from the complex and to impair recruitment of ULK1 to the phagophore assembly site (PAS).

The direct interaction of ATG13 and ULK1 and the recruitment of ULK1 to the autophagy-initiating complex are not necessarily required for autophagy

Next we addressed the question of whether the presence of ULK1 within the ~3 MDa complex is essential for autophagy induction upon starvation. For this purpose, we stably transfected differently reconstituted *Atg13* KO MEFs with cDNA encoding mCitrine-MAP1LC3/LC3 and analyzed lysosomal degradation of mCitrine-LC3 upon starvation by flow cytometry. In wild-type MEFs and *Atg13* KO MEFs reconstituted with wild-type HA-ATG13, HA-ATG13$^{1AA\Delta}$, or HA-ATG13^{F429A,F433A} incubation in EBSS resulted in strong lysosome-dependent degradation of mCitrine-LC3, which in turn was blocked by addition of bafilomycin A_1 (**Fig. 4A**). In contrast, EBSS-induced degradation of mCitrine-LC3 did not occur in *Atg13* KO MEFs. Of note, in MEFs expressing HA-ATG13$^{2AA\Delta}$, HA-ATG13$^{3AA\Delta}$, or HA-ATG13$^{57AA\Delta}$ the autophagic degradation of mCitrine-LC3 was clearly reduced, but not completely absent (**Fig. 4A**). Generally, these observations confirmed previous results establishing the importance of the ULK1/2-ATG13 interaction for autophagy induction[3,4,6,7] but apparently some autophagic activity remains even in the absence of this interaction. We also investigated LC3B turnover in *Atg13* KO MEFs transfected with empty vector or cDNA encoding either full-length HA-ATG13 or HA-ATG13$^{3AA\Delta}$ by immunoblotting. LC3B-I and -II levels remained unaltered in control-transfected *Atg13* KO MEFs upon EBSS treatment (**Fig. 4B**). Interestingly, autophagy was induced in both HA-ATG13- and HA-ATG13$^{3AA\Delta}$-expressing cells as detected by increased LC3B-II levels in EBSS/bafilomycin A_1-treated cells compared to DMEM-bafilomycin A_1-treated cells (**Fig. 4B**). Similar observations were made for SQSTM1/p62, which bridges LC3 and ubiquitinated substrates and thus serves as readout for autophagic degradation.[24] SQSTM1 accumulation observed in *Atg13* KO MEFs was absent in both HA-ATG13- and HA-ATG13$^{3AA\Delta}$-expressing MEFs (**Fig. 4B**). Furthermore, ULK1 stabilization was evident only in HA-ATG13-expressing cells, whereas *Atg13* KO and HA-ATG13$^{3AA\Delta}$-expressing MEFs depicted clearly reduced ULK1 levels (**Fig. 4B**). In turn, ATG101 was stabilized by both ATG13 variants (**Fig. 4B**). These ATG13-dependent effects on ULK1 and ATG101 expression levels were already apparent in the size exclusion analyses described above (**Fig. 2**). We also analyzed phosphorylation of ATG13 Ser318, which has been previously identified as ULK1-dependent phospho-acceptor site during mitophagy.[25] While we observed a clear increase in Ser318 phosphorylation in HA-ATG13-expressing cells upon EBSS treatment, this was not the case in cells expressing the ULK1 binding-deficient HA-ATG13$^{3AA\Delta}$ variant (**Fig. 4B**). This data suggest that 1) a direct interaction between ULK1 and ATG13 is necessary for Ser318 phosphorylation and 2) phosphorylation of this site is not absolutely required for starvation-induced autophagy. The latter was confirmed by expression of a Ser318-to-Ala (S318A) ATG13 mutant in *Atg13* KO MEFs, which mounts a normal autophagic response (data not shown). In summary, the mCitrine-LC3 degradation assay clearly supported the importance of the ULK1-ATG13 interaction for starvation-induced autophagy. However, both the mCitrine-LC3 degradation assay and the LC3 turnover assay suggest that the ULK1 binding-deficient ATG13 variants can at least partially restore autophagic activity. To further elucidate this latter aspect, we performed immunofluorescence of endogenous LC3B and SQSTM1 (**Fig. 5**). *Atg13* KO MEFs showed almost no increased LC3B puncta formation upon starvation and bafilomycin A_1 treatment (**Fig. 5A**, upper panels). MEFs reconstituted with full-length HA-ATG13 showed formation of LC3B-positive structures upon starvation, which could be further increased by addition of bafilomycin A_1 (**Fig. 5A**, middle panels). HA-ATG13$^{3AA\Delta}$-expressing MEFs revealed a similar tendency, although overall LC3 puncta numbers were reduced in cells incubated in DMEM or EBSS compared to full-length ATG13-expressing MEFs (**Fig. 5A**, lower panels). Again, analogous observations were made for SQSTM1. *Atg13* KO MEFs did not show a prominent

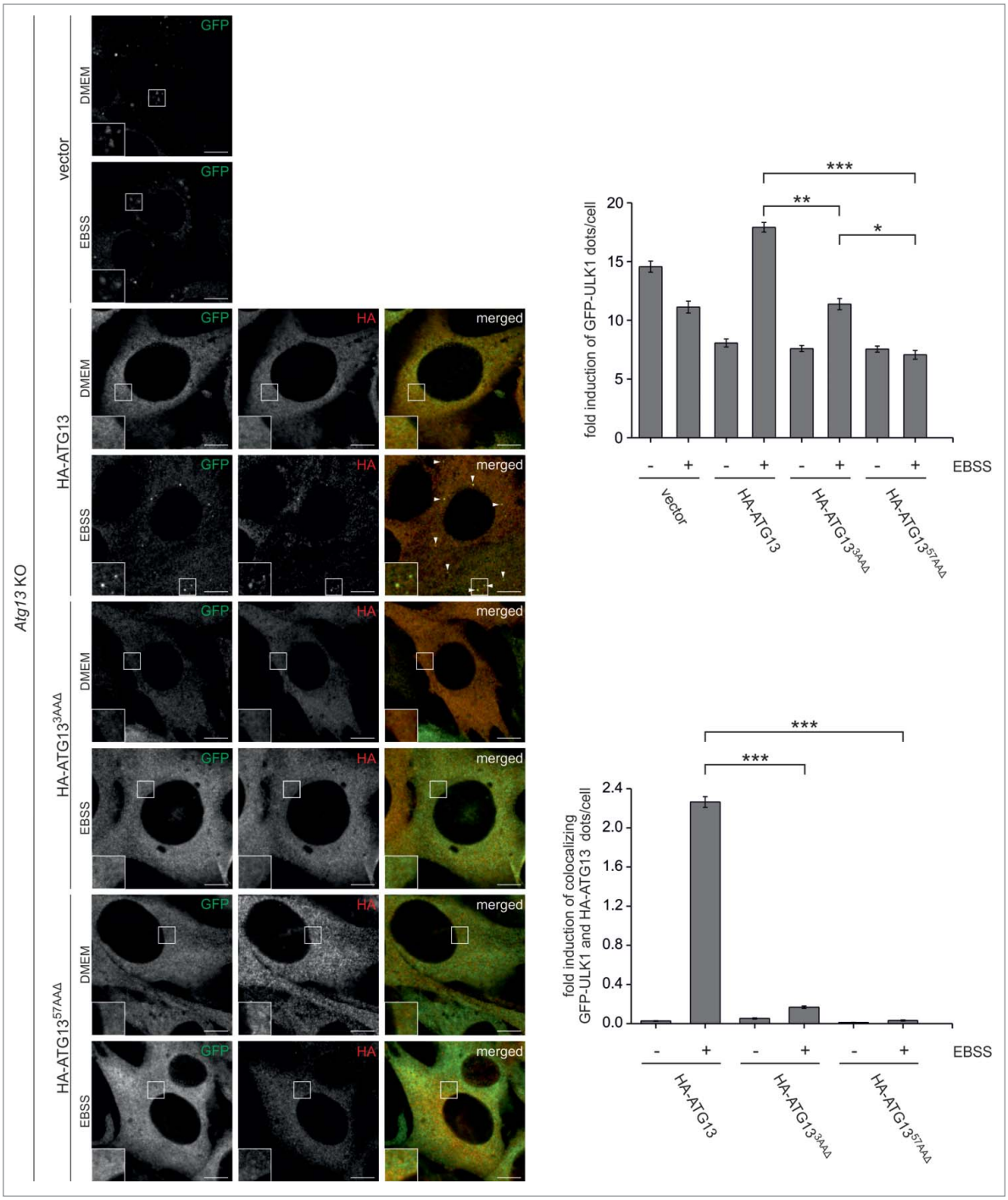

Figure 3. ULK1 does not localize with ULK1 binding-deficient variants of ATG13. GFP-ULK1-expressing *Atg13* KO MEFs retrovirally transfected with empty vector or cDNA encoding HA-ATG13, HA-ATG13$^{3AA\Delta}$ or HA-ATG13$^{57AA\Delta}$ were cultured in regular medium or starvation medium (EBSS) for 2 h. Cells were fixed and analyzed by immunofluorescence microscopy using anti-GFP and anti-HA antibodies. Scale bar: 10 μm. The number of GFP-ULK1 dots and colocalization of GFP-ULK1 and HA-ATG13 dots were quantified from at least 220 cells using Fiji software and data represent mean ± SEM. *$P < 0.05$, **$P < 0.01$, ***$P < 0.001$ (Student *t* test, 2-sample assuming unequal variances).

increase in SQSTM1-positive structures upon EBSS treatment in the presence of bafilomycin A_1, whereas this was clearly the case for both cell lines expressing the 2 different ATG13 variants (**Fig. 5B**). In order to more robustly analyze the autophagic flux, we generated cell lines stably expressing the tandem fluorescent mRFP-EGFP-LC3B chimeric protein for the detection of early and late autophagic activity.[26] In *Atg13* KO MEFs, only mRFP-EGFP-double-positive structures, which may represent protein aggregates generated under autophagy-deficient conditions, were detectable upon starvation for 2 h, whereas both reconstituted

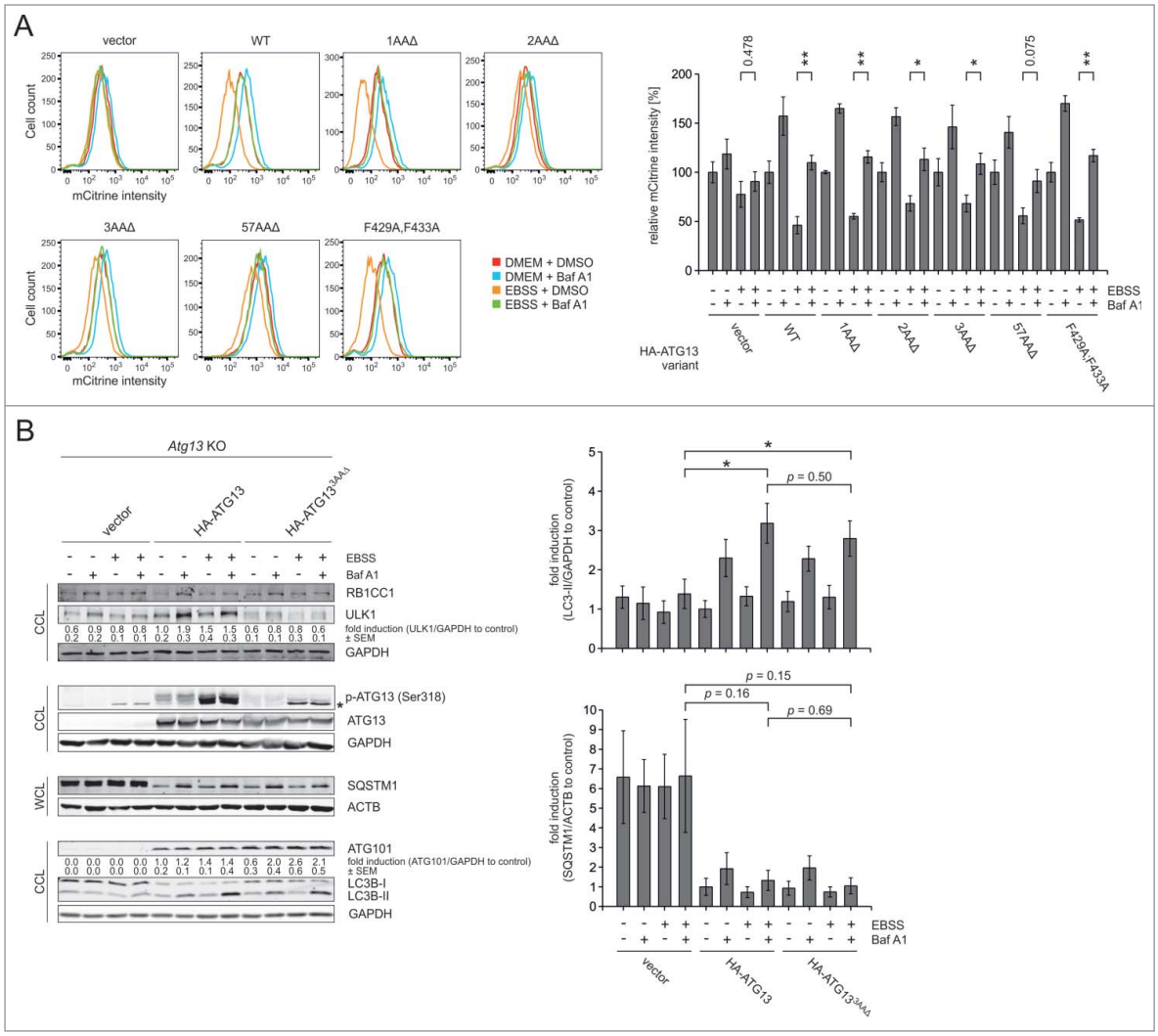

Figure 4. ATG13$^{3AA\Delta}$ supports mCitrine-LC3 degradation in *Atg13* KO MEFs but does not support ULK1 stabilization. (**A**) MEFs stably expressing mCitrine-LC3 and the indicated ATG13 variants were cultured in regular medium or starvation medium (EBSS) with or without 40 nM bafilomycin A_1 (Baf A1) for 10 h. Total cellular mCitrine-LC3 signals were analyzed by flow cytometry. Cell debris was eliminated by gating. Representative FACS data from 3 independent experiments is shown in the panels. The median of fluorescence intensity was plotted in a bar diagram. Values are expressed as a percentage of the mean of cells cultured in regular medium. Data represent mean ± SEM. $^*P < 0.05$, $^{**}P < 0.01$ (Student *t* test, 2-sample assuming unequal variances). (**B**) *Atg13* KO MEFs retrovirally transfected with empty vector or cDNA encoding HA-ATG13 or HA-ATG13$^{3AA\Delta}$ were incubated in culture medium (DMEM) or starvation medium (EBSS) in the presence or absence of 40 nM bafilomycin A_1 for 2 h. Cells were lysed and lysates (either cleared cellular lysates, CCL, or whole cellular lysates, WCL) were subjected to immunoblotting for RB1CC1, ULK1, phospho-ATG13 (Ser318), ATG13, SQSTM1/p62, ATG101, LC3B, ACTB, and GAPDH. Asterisk indicates a nonspecific background band. Data shown are representative of at least 3 independent experiments. Fold changes were calculated by dividing each normalized ratio (protein to loading control) by the average of the ratios of the control lane (HA-ATG13 + DMEM, n ≥ 3). Results are mean ± SEM and are given below the corresponding blots (ULK1 and ATG101) or are plotted as bar diagram (LC3-II and SQSTM1/p62). $^*P < 0.05$, $^{**}P < 0.01$ (Student *t* test, 2-sample assuming unequal variances).

MEF cell lines revealed mRFP-single-positive structures presumably representing autolysosomes (**Fig. 6A**). Finally, we performed a long-lived protein degradation assay. Although statistically not significant, it again appeared that the ATG13$^{3AA\Delta}$ variant can partially compensate the autophagy-defective phenotype of *Atg13* KO MEFs (**Fig. 6B**).

In the past, several noncanonical autophagy signaling pathways have been proposed, including ULK1/2-, BECN1/VPS30-PIK3C3/VPS34- and ATG5-ATG7-independent processes.[20,27,28] Since the majority of our autophagy readouts were based on LC3 lipidation, we can exclude ATG5-ATG7-independent effects. However, we investigated whether the partial restoration of autophagy observed for ATG13$^{3AA\Delta}$-expressing MEFs depends on ULK1/2 or the PtdIns3K class III complex. The observation that autophagic flux can partially be restored independent of the ULK1-ATG13 interaction does not necessarily imply that the process is ULK1/2-independent. We performed *Ulk1/2* RNAi experiments in *Atg13* KO MEFs transfected with empty vector or cDNA encoding either full-length HA-ATG13 or HA-ATG13$^{3AA\Delta}$ and analyzed LC3 turnover by immunoblotting (**Fig. S4A**). However,

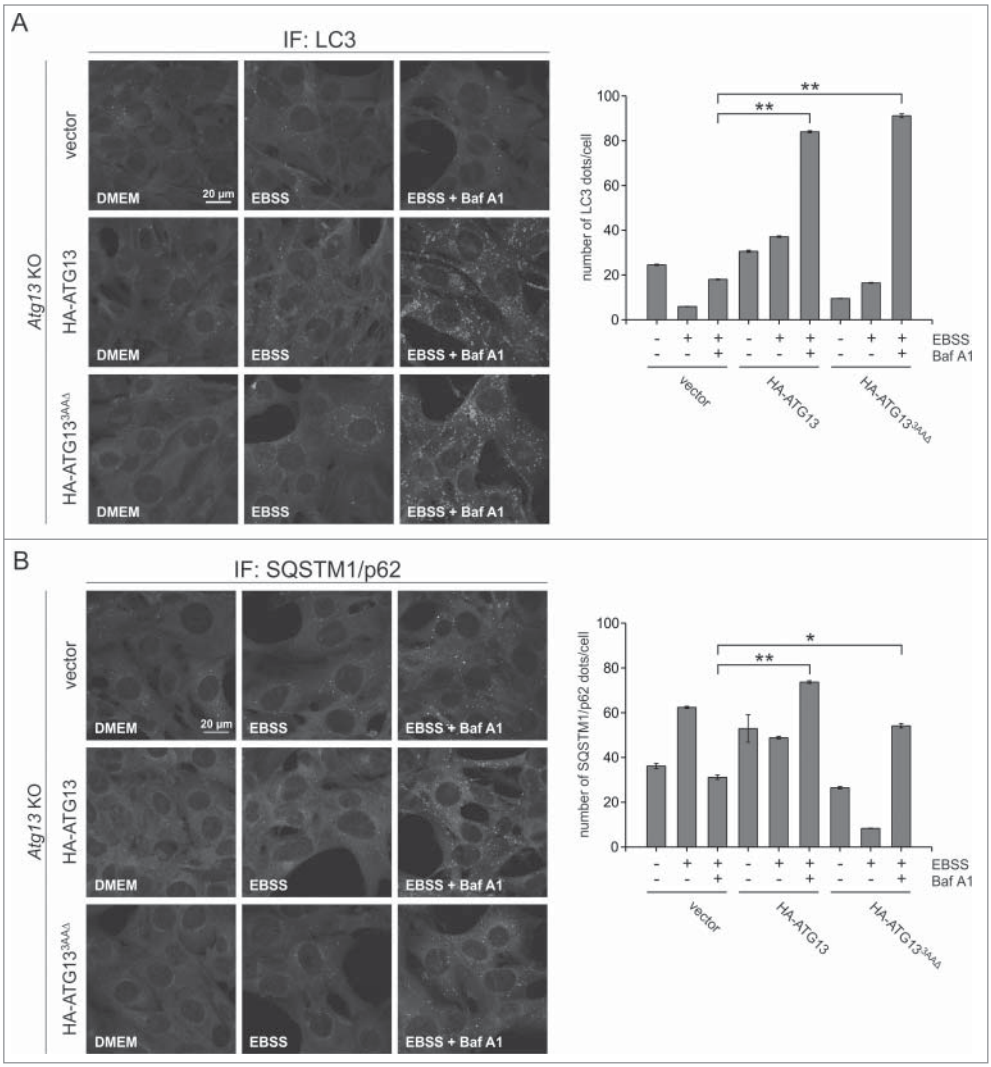

Figure 5. ATG13$^{3AA\Delta}$ supports starvation-induced accumulation of LC3 and SQSTM1/p62 puncta in the presence of bafilomycin A_1 in *Atg13* KO MEFs. (**A and B**) *Atg13* KO MEFs retrovirally transfected with empty vector or cDNA encoding full-length HA-ATG13 or HA-ATG13$^{3AA\Delta}$ were grown on glass coverslips for 24 h and then incubated in culture medium (DMEM) or starvation medium (EBSS) in the presence or absence of 40 nM bafilomycin A_1 for 2 h. Cells were fixed and LC3B (**A**) or SQSTM1/p62 (**B**) were detected by confocal laser-scanning microscopy. Fiji software was used to process and count the puncta. At least 505 cells were scored for each condition. Data represent mean ± SEM. $^*P < 0.05$, $^{**}P < 0.01$ (Student *t* test, 2-sample assuming unequal variances).

from these results, it is difficult to interpret the relevance of ULK1. This is in line with observations made in *Ulk1/2* DKO MEFs, in which LC3-II levels clearly increase upon starvation (ref,[29] and own observation). With regard to the PtdIns3K class III complex, we pursued 2 approaches. First we used *Becn1* siRNA similar to the experiments described above (**Fig. S4B**). Since BECN1 knockdown efficiency appeared to be insufficient, we employed the PtdIns3K class III inhibitor 3-methyladenine (3-MA). 3-MA blocked autophagy in both HA-ATG13- or HA-ATG13$^{3AA\Delta}$-expressing MEFs (**Fig. S4C**), indicating that PtdIns3K class III activity is important for the observed phenomenon.

Taken together, our results suggest that autophagy induction depends on the interaction between ULK1/2 and ATG13—which is mediated by a short C-terminal motif of ATG13—but that autophagic capacity can be partially restored by the ULK1/2 binding-deficient variant of ATG13. Apparently, this remaining autophagic competence depends on the core autophagy signaling machinery, i.e. the PtdIns3K class III complex and the LC3-conjugation system.

Discussion

The mammalian ULK1/2-ATG13-RB1CC1-ATG101 complex is essential for the initiating steps of autophagy. In recent years, the molecular details of how this complex regulates autophagy have been deciphered. It is generally accepted that the complex is constitutively assembled, independently of nutrient supply. It has been proposed that the proautophagic activity of the ULK1/2 complex is mainly controlled by the upstream kinases MTOR, PRKA/AMPK, or AKT. Here, we identified a short ULK1/2 binding motif at the C terminus of ATG13, which is composed of the last 3 amino acids TLQ480. Furthermore, we demonstrated that this motif is essential for the recruitment of ULK1 into the autophagy-regulating complex and to the PAS. Although lysosomal degradation of mCitrine-LC3 was slightly compromised in cells expressing the C-terminal truncated version of ATG13, we surprisingly observed that the direct association of ULK1/2 with ATG13 is not absolutely required to support the induction of autophagy.

Our data reveal that the last 3 amino acids of ATG13 represent or at least contribute to the core interaction site for ULK1/2. Thus, we clearly fine-mapped the ULK1-interaction site, which has been previously mapped to amino acids 384 to 517 (amino acid numbering of human isoform 1; corresponds to amino acids 347 to 480 of human isoform 2).[7] In our view, there exist 2 possibilities how the last 3 amino acids of ATG13 might mediate ULK1/2 binding: 1) these amino acids represent the direct binding site for ULK1/2, or 2) these amino acids are structurally relevant for the ULK1/2 binding site. With regard to the first

possibility, short peptide motifs at the C terminus of proteins are bound by PDZ (postsynaptic density 95, PSD-95; discs large, Dlg; zonula occludens-1, ZO-1) domains.[30-32] Of note, it has been proposed that ULK1 itself harbors a PDZ binding motif at its C terminus.[6,33,34] However, the C terminus of ULK1 is not very conserved across species, and the reported YVA motif in murine ULK1 cannot be found in human ULK1. In contrast, the TLQ480 motif of ATG13 is highly conserved across vertebrate species (including *H. sapiens, M. musculus, G. gallus, F. catus, C. familiaris, B. taurus, D. rerio*), resembles a class I PDZ domain ligand,[30,32,35] and binding specificity might be regulated by phosphorylation of Thr478. Indeed, we have previously proposed that Thr478 might be a ULK1-dependent phospho-acceptor site.[9] However, mutation of Thr478 to either phospho-deficient alanine or phospho-mimicking glutamic acid did not modulate ULK1 binding (data not shown). Furthermore, ULK1/2 has not been characterized as PDZ-domain-containing protein so far. Nevertheless, it is tempting to speculate that the C-terminal peptide motif of ATG13 represents a PDZ-domain binding ligand. Alternatively, the last 3 amino acids are structurally important for the ULK1/2 binding site. Fujioka et al. have reported the X-ray crystallographic analysis of the interaction of yeast Atg13 with Atg1 and Atg17.[23] Atg13 binds tandem microtubule interacting and transport (tMIT) domains in Atg1 via a 2-part MIT-interacting motif. These Atg1 binding regions in Atg13 have been recently confirmed by hydrogen-deuterium exchange coupled to mass spectrometry.[36] Fujioka et al. suggest that the MIT-MIM interaction is conserved in mammals, and ULK1 was purified by a GST fusion protein comprising the last 60 amino acids of ATG13. According to the authors, the C-terminal half of the MIM domain is established by the amino acids of the ATG13 C terminus.[23] Thus, it is also feasible that the deletion of the TLQ480 motif disrupts the structure of the MIM domain, ultimately abolishing the interaction with ULK1. Fujioka et al. suggest that Phe429 and Phe433 are part of the N-terminal half of the MIM domain of the mammalian ATG13. However,

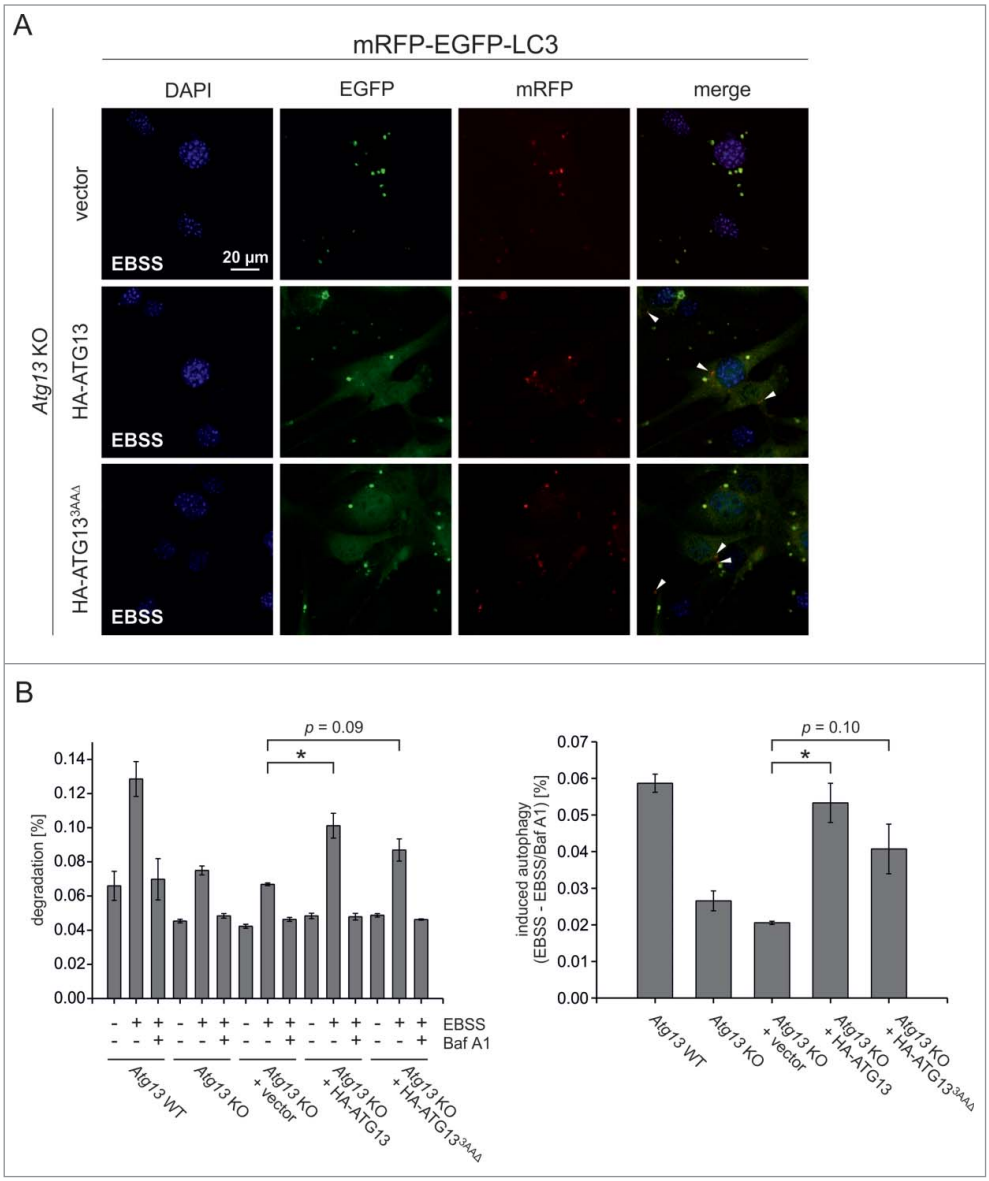

Figure 6. ATG13$^{3AA\Delta}$ can partially restore autophagic flux in *Atg13* KO MEFs and supports long-lived protein degradation. (**A**) *Atg13* KO MEFs retrovirally transfected with empty vector or cDNA encoding full-length HA-ATG13 or HA-ATG13$^{3AA\Delta}$ were additionally retrovirally transfected with pMSCVblast/mRFP-EGFP-rLC3. Cells were incubated in starvation medium (EBSS) for 2 h, fixed, and analyzed by confocal laser scanning microscopy. Autolysosomes are indicated by white arrow heads. (**B**) Cellular proteins of the indicated MEF cells were labeled with L-[^{14}C]valine as described in the Materials and Methods section. Cells were washed and treated with the indicated medium (control or EBSS ± Baf A1) for 4 h. For each sample, the radioactivity of the acid-soluble fraction of the medium and the radioactivity in the cells remaining in the well were measured. Percent degradation was assessed as the acid-soluble radioactivity of the medium divided by the total radioactivity (left diagram). Additionally, induction of autophagy was assessed by subtracting percent degradation of EBSS/Baf A1-treated cells from percent degradation of EBSS-treated cells (right diagram). Data shown are mean of triplicates of averaged duplicates ± SEM; *$P < 0.05$ (Student *t* test, 2-sample assuming unequal variances).

mutation of these 2 phenylalanine residues to alanine did not impair ATG13 function in our analyses. Collectively, future experiments and structural analyses will have to reveal the existence of a MIM domain in mammalian ATG13 and the exact function of the TLQ480 motif.

In the recent past, several ULK1-interacting partners have been identified which might contribute to the recruitment of ULK1 to the PAS. For example, it has been suggested that ULK1 might interact directly with RB1CC1.[3] The authors used recombinant proteins in an in vitro binding assay. In contrast, Jung et al. and Hosokawa et al. see a prominent dependency on ATG13 for the ULK1-RB1CC1 interaction,[4,7] which corresponds to our observations. The ATG13$^{3AA\Delta}$ protein retains normal RB1CC1 binding, but ULK1 cannot be purified by affinity purification or immunopurification with this truncated protein. Furthermore, ULK1 and RB1CC1 cannot be coimmunopurified from lysates of *Atg13* KO MEFs. The same holds true for a potential interaction between ULK1 and ATG101, which has been suggested for the *C. elegans* orthologs UNC-51/ATG-1 and EPG-9/ATG-101.[37] Whereas these results might be explained by our cell lysis conditions (0.3% CHAPS), we additionally showed 1) by size exclusion chromatography that ULK1 is not part of the high molecular mass complex in HA-ATG13$^{3AA\Delta}$-expressing MEFs and 2) by confocal microscopy that GFP-ULK1 is not efficiently recruited to the PAS in these MEFs. Collectively, our data do not support the hypothesis that ULK1 is recruited to the PAS in general and to the high molecular mass complex in particular via direct interaction with RB1CC1 or ATG101, respectively. Similarly, we assume that previously reported alternative "PAS recruitment options"—i.e. via protein binding to ATG8 proteins or via direct lipid binding—play only a minor role compared to the direct ULK1-ATG13 interaction. Admittedly, we cannot entirely exclude that a transient or low-affinity interaction between ULK1 and ATG13$^{3AA\Delta}$ might support autophagy induction. Our affinity/immunopurification experiments and the size exclusion experiments are in vitro approaches and depend on the overexpression of at least one of the 2 components. However, some of our observations clearly show that the association between ULK1 and the ATG13 mutants is severely compromised, e.g. the missing stabilization of ULK1 by ATG13$^{3AA\Delta}$ or the absent colocalization of these 2 proteins as detected by immunofluorescence.

We employed different readout methods to analyze autophagy in cells expressing the TLQ-deleted variant of ATG13. Although these assays confirm the importance of the ULK1-ATG13 interaction for autophagy induction, it appears that autophagic activity is at least partially restored in ATG13$^{3AA\Delta}$-expressing cells. Our results likely reflect that starvation-induced autophagy cannot entirely be blocked by the disruption of the ULK1/2-ATG13 interaction. In general, 2 mechanisms might explain the observed restoration of autophagic activity by ATG13$^{3AA\Delta}$: 1) ULK1/2-independent autophagy pathways or 2) ULK1/2-dependent but ULK1/2-ATG13 interaction-independent autophagy pathways. So far, we cannot easily distinguish between these 2 possibilities. It has been previously shown that amino acid starvation-induced autophagy is largely blocked in ULK1/2 double-deficient MEFs, indicating that this autophagic pathway requires ULK1/2 activity.[20,29] However, McAlpine et al. state that detectable levels of amino acid starvation-induced autophagy in form of LC3 lipidation are still observable following double knockout of ULK1/2.[29] This is in accordance with our own observations (data not shown). Additionally, ULK1/2-independent autophagy has been proposed for other stimuli (i.e. glucose starvation) or other cellular systems (i.e. chicken DT40 B lymphocytes).[9,20] We performed *Ulk1/2* siRNA experiments in ATG13$^{3AA\Delta}$-expressing cells and analyzed LC3 turnover. However, so far we cannot convincingly determine the functional role of ULK1 for the partial autophagic flux. In order to clarify this issue, one approach would be the reconstitution of *Ulk1, Ulk2*, and *Atg13* triple-knockout cells with single components. What we can say so far is that the partial autophagic flux in ATG13$^{3AA\Delta}$-expressing cells depends on other conventional autophagy signaling modules, i.e. the BECN1-PIK3C3 complex and the LC3 conjugation system.

Collectively, our data challenge the current view of a constitutively assembled ULK1/2 complex as unequivocal requirement for autophagy induction. Future experiments will have to reveal the relative contribution of pathways dependent or independent of the ULK1/2-ATG13 interaction to autophagy. Furthermore, one might speculate that different (selective) autophagic processes might vary in their dependency on this interaction. Interestingly, Joo et al. reported that mitochondrial damage triggers ULK1 activation and ULK1-dependent phosphorylation of ATG13, which then leads to the release of ATG13 and its translocation to the damaged mitochondria.[25] These data suggest a phosphorylation-dependent regulation of the ULK1-ATG13 interaction during selective autophagy processes. Finally, Kraft et al. report for the yeast orthologs that the autophagy defects of an Atg1 binding-deficient Atg13 mutant are less pronounced than the defects of a complete Atg13 knockout,[38] similarly indicating a differential requirement for this interaction. Although the majority of the relevant components of this autophagy-initiating complex are identified, apparently the molecular dynamics of their interplay are far from being completely understood.

Materials and Methods

Antibodies and reagents

Antibodies against ACTB/β-actin (clone AC-74, Sigma-Aldrich, A5316), ATG101 (Sigma-Aldrich, SAB4200175), ATG13 (Sigma-Aldrich, SAB4200100), ATG13 pSer318 (Rockland Immunochemicals, 600-401-C49), GAPDH (clone 6C5, Abcam, ab8245), GFP (Roche, 11814460001, ChromoTek, 3h9, and Nacalai Tesque, 04404-84), GST (GE Healthcare, 27-4577-01), HA (Covance, MMS-101R), HSPA1A/B (BD Transduction Laboratories, 610607), LC3B (Cell Signaling Technology, 2775, and MBL International, PM036), RB1CC1 (Bethyl Laboratories, A301-536A), SQSTM1/p62 (MBL, PM045, and PROGEN Biotechnik, GP62-C), and ULK1 (clone D8H5, Cell Signaling Technology, 8054, or Sigma-Aldrich, A7481) were used. Alternatively, antibodies for ATG101 and RB1CC1 have been previously described.[5,22] IRDye 800- or IRDye 680-

conjugated secondary antibodies were purchased from LI-COR Biosciences (926-32210/11, 926-68070/71, 926-68024 and 926-32214), Alexa Fluor® 488-conjugated goat anti-rat IgG (H^+L) antibodies and Alexa Fluor® 568-conjugated goat anti-mouse IgG (H^+L) antibodies from Life Technologies (A-11006 and A-11031), and Alexa Fluor® 647-conjugated goat anti-rabbit IgG (H^+L) antibodies from Jackson ImmunoResearch Laboratories (111-605-003). Bafilomycin A_1 was obtained from Sigma-Aldrich (B1793). [^{14}C]Valine (NEC291EU050UC) was purchased from PerkinElmer.

Cell lines and cell culture

Wild-type and *Atg13* KO MEFs were kindly provided by Xiaodong Wang.[14] Generation of Flp-In™ T-REx™ 293 cells inducibly expressing GFP-ULK1 or GFP-ULK1$^{CTD\Delta}$ was previously described.[39] The vector pcDNA5/FRT/TO-GFP containing human *ULK2* cDNA was kindly provided by Dario Alessi. This vector was cotransfected with pOG44 (Life Technologies, V6005-20) into Flp-In™ T-REx™ 293 cells (Life Technologies, R780-07). Stable transfectants were selected with 200 μg/ml hygromycin B (Life Technologies, 10687-010) and 5 μg/ml blasticidin (Life Technologies, A11139-02). MEFs and Flp-In™ T-REx™ 293 cell lines were cultured in DMEM (4.5 g/l D-glucose) supplemented with 10% FCS, 100 U/ml penicillin and 100 μg/ml streptomycin (PAA Laboratories GmbH, E15-810) in a 5% CO_2 humidified atmosphere at 37°C. For induction of GFP-ULK1/2 expression, Flp-In™ T-REx™ 293 GFP-ULK1/2 cells were stimulated with 0.1 μg/ml doxycycline (Clontech, 631311) for 4 to 6 h. For starvation treatment, cells were washed with Earle's Balanced Salt Solution (EBSS, Gibco, 24010-043) and incubated in EBSS for the indicated time periods.

Expression constructs and transfections

pEGB-6P/ATG13 (human isoform 2) and pEGB-6P/3AAΔ were kindly provided by Dario Alessi (MRC Protein Phosphorylation Unit, College of Life Sciences, University of Dundee, UK). All other pEGB-6P/ATG13 variants were generated by site-directed mutagenesis. Transient transfection of Flp-In™ T-REx™ 293 cells with pEGB-6P vectors was performed using Lipofectamine™ 2000 or Lipofectamine™ 3000 (Life Technologies, 11668019 and L3000015). Human cDNAs encoding either HA-tagged full-length ATG13 (isoform 2) or ATG13 mutants were cloned into pMSCVpuro (Clontech Laboratories, Takara Bio, 631461) for retroviral infection of MEFs. pMSCVblast/GFP-ULK1 was generated by cloning *GFP-ULK1* cDNA from pcDNA5/FRT/TO-GFP-ULK1 (previously described in ref. 39) into pMSCVblast, which was generated by replacing the puromycin resistance cassette of pMSCVpuro by a blasticidin resistance cassette amplified from pcDNA™6/TR (Life Technologies, V1025-20). To generate pMSCVblast/mCitrine-LC3 plasmid, the cDNA encoding human LC3 was subcloned into pMSCVblast together with mCitrine. pMSCVblast/mRFP-EGFP-rLC3 expression vector was generated by cloning of m*RFP-EGFP-rLC3* cDNA from pmRFP-EGFP-rLC3 (kindly provided by Tamotsu Yoshimori, Department of Genetics, Osaka University Graduate School of Medicine, Japan) into pMSCVblast. For the production of recombinant retroviruses, Plat-E cells (kindly provided by Toshio Kitamura, Institute of Medical Science, University of Tokyo, Japan) were transfected with pMSCVpuro- or pMSCVblast-based retroviral vectors using FuGENE® 6 or FuGENE® HD transfection reagent (Roche, 11988387001 and 04709713001). *Atg13* KO MEF cells were incubated with retroviral supernatant fractions containing 3 to 8 μg/ml Polybrene (Sigma-Aldrich, H9268-106) and selected in medium containing 2.5 μg/ml puromycin (InvivoGen, ant-pr-1) or 35 μg/ml blasticidin (InvivoGen, ant-bl-1).

Affinity and immunopurification and immunoblotting

Cells were lysed in lysis buffer (50 mM Tris-HCl, pH 7.5, 150 mM NaCl, 0.3% [v/v] CHAPS [Carl Roth GmbH + Co. KG, 1479.3] or 1% Triton X-100 [Carl Roth GmbH + Co. KG, 3051.2], 1 mM EDTA, 1 mM EGTA, 1 mM Na_3VO_4, 50 mM NaF, 5 mM $Na_4P_2O_7$, 0.27 M sucrose [Carl Roth GmbH + Co. KG, 4621.1], protease inhibitor cocktail [Sigma-Aldrich, P2714]) for 30 min on ice. Lysates were flash frozen and/or directly clarified by centrifugation at 17,000 *g* for 15 min at 4°C. Equal protein amounts were determined by Bradford method. Alternatively, whole cell lysates were prepared by direct addition of sample buffer (125 mM Tris-HCl, pH 6.8, 17.2% [v/v] glycerol, 4.1% [w/v] SDS [AppliChem GmbH, A7249], 200 μg/ml bromophenol blue, 2% [v/v] β-mercaptoethanol) to the cells and subsequent sonification. Lysates were subjected to 6–15% SDS-PAGE. Proteins were transferred to PVDF membranes (Merck, Millipore, IPFL00010) and immunoblot analysis was performed using the indicated primary antibodies and appropriate IRDye®800- or IRDye®680-conjugated secondary antibodies (LI-COR Biosciences). Signals were detected with an Odyssey® Infrared Imaging system (LI-COR Biosciences). For affinity or immunopurification of GST-, GFP- or HA-tagged proteins, clarified lysates were incubated with either glutathione sepharose 4B beads (GE Healthcare, 17-0756-01), GFP-trap® beads (ChromoTek, gta-200) or monoclonal anti-HA agarose beads (clone HA-7, Sigma-Aldrich, A2095) at 4°C for 1.5 to 3 h or overnight with rotation. For immunopurification of untagged proteins, clarified lysates were incubated with corresponding antibodies and protein A and G sepharose (GE Healthcare, 17-5280-01 and 17-0618-01) mixed in equal parts at 4°C overnight. Purified proteins were washed at least 3 times with lysis buffer and analyzed by immunoblotting.

Size-exclusion chromatography

MEFs were lysed in a hypotonic buffer (40 mM Tris HCl, pH 7.5, and Complete EDTA-free protease inhibitor cocktail [Roche, 0505648900]) by repeated passages (15 times) through a 1-ml syringe with a 27-gauge needle and incubation on ice for 20 min following addition of NaCl to a final concentration of 150 mM. The homogenates were centrifuged at 13,000 × *g* for 15 min, and the supernatant fractions were further centrifuged at 100,000 × *g* for 60 min. The supernatant fractions (S100 fractions) were then filtered with Ultrafree-MC 0.45-μm filter unit (Millipore, UFC30HV00) and applied to a Superose 6 column

(GE Healthcare, 17-5172-01). Subsequently, 0.5-ml fractions were collected at a flow rate of 0.5 ml/min with elution buffer (40 mM Tris-HCl, pH 7.5, 150 mM NaCl). The fractions were then analyzed by immunoblotting. The column was calibrated with thyroglobulin (669 kDa), ferritin (440 kDa), catalase (240 kDa), and ovalbumin (43 kDa).

Confocal laser scanning microscopy

For immunofluorescent staining of LC3B and SQSTM1/p62, cells were grown on glass coverslips overnight, stimulated as indicated and fixed in 4% formaldehyde solution, following incubation with primary antibodies overnight and secondary antibodies for 1 h in 0.05% saponin (Sigma-Aldrich, 47036) in phosphate-buffered saline (Gibco, 14190-094). Subsequently, cells were stained with 1 μg/ml DAPI (Carl Roth GmbH + Co. KG, 6335.1) and embedded in Mowiol 4-88 (Carl Roth GmbH + Co. KG, 0713.1). MEF cells stably expressing mRFP-EGFP-rLC3B were stained with DAPI only. Samples were analyzed on a Leica TCS SP2 confocal laser-scanning microscope (Wetzlar, Germany). For immunofluorescent staining of GFP-ULK1 and HA-ATG13, cells were grown on glass coverslips, stimulated as indicated and fixed in 4% formaldehyde solution, permeabilized with 50 μg/ml digitonin (Wako, 043-21376) in phosphate-buffered saline (Gibco, 14200-075), and stained with anti-GFP rat monoclonal antibodies and anti-HA mouse monoclonal antibodies. As secondary antibodies Alexa Fluor® 488-conjugated anti-rat IgG and Alexa Fluor® 568-conjugated anti-mouse IgG antibodies were used. Samples were analyzed with a confocal laser microscope (FV1000D; Olympus, Tokyo, Japan) using a 60x PlanApoN oil immersion lens (1.42 NA; Olympus). DAPI was excited at 405 nm, EGFP or Alexa Fluor® 488 at 488 nm, Alexa Fluor® 568 at 559 nm, mRFP at 594 nm and Alexa Fluor® 647 at 633 nm wavelengths.

Flow cytometry

Cells stably expressing mCitrine-LC3 were cultured in the indicated medium for 10 h, harvested with 0.05% trypsin-EDTA, and washed once with phosphate-buffered saline. The samples were analyzed using an LSRFortessa flow cytometer (Becton Dickinson, Heidelberg, Germany).

Long-lived protein degradation assay

Cells were incubated for 72 h with 0.125 μCi/ml L-[^{14}C] valine-supplemented medium, followed by 2 washes and a 16 h chase in fresh medium containing 10 mM nonradioactive L-valine to allow degradation of short-lived proteins. Next, the cells were washed and treated with the indicated medium for 4 h. For each sample, the radioactivity of the acid-soluble fraction of the medium and the radioactivity in the cells remaining in the well were measured.

Statistical analysis

For western blotting, fold changes were calculated by dividing each normalized density ratio (protein of interest to loading control) by the average of the density ratios of the control lane (control lane: fold change = 1.00, n ≥ 3). Results are mean ± SEM and are given below the corresponding blots or are depicted in a bar diagram. For GFP-ULK1, HA-ATG13, LC3B and SQSTM1/p62 immunofluorescence, the number of GFP-ULK1 dots, LC3B dots, SQSTM1 dots and colocalizing GFP-ULK1 and HA-ATG13 dots were quantified from at least 220 cells using Fiji software and data represent mean ± SEM. For mCitrine-LC3B degradation, data represent the mean of the median fluorescence intensity (5,000 cells/experiment; 3 independent experiments) ± SEM. Values are expressed as a percentage of the mean of cells cultured in regular medium (DMEM without bafilomycin A_1). For the long-lived protein degradation assay, the radioactivity of the acid-soluble fraction of the medium and the radioactivity in the cells remaining in the well were measured for each sample. Percent degradation was assessed as the acid-soluble radioactivity of the medium divided by the total radioactivity. Additionally, induction of autophagy was assessed by subtracting percent degradation of EBSS/Baf A1-treated cells from percent degradation of EBSS-treated cells. Data shown are mean of triplicates of averaged duplicates ± SEM and are depicted in bar diagrams. For all analyses, P values were determined by the Student t test (2-samples, unequal variances) and the significance levels were set as follows: * indicates $P < 0.05$, ** indicates $P < 0.01$, *** indicates $P < 0.001$.

Disclosure of Potential Conflicts of Interest

No potential conflicts of interest were disclosed.

Acknowledgments

We thank Toshio Kitamura for providing Plat-E cells, Dario Alessi for providing pEGB-6P/ATG13, pEGB-6P/ATG13$^{3AA\Delta}$ and pcDNA5/FRT/TO-GFP-ULK2, Tamotsu Yoshimori for providing pmRFP-EGFP-rLC3, and Xiaodong Wang for providing wild-type and *Atg13* KO MEFs.

Funding

This work was supported by the Deutsche Forschungsgemeinschaft STO 864/3-1 and STO 864/4-1 (to B.S.), the Research Committee of the Medical Faculty of the Heinrich-Heine-University Düsseldorf 58/2013 (to B.S.), the Düsseldorf School of Oncology (to S.W. and B.S.; funded by the Comprehensive Cancer Center Düsseldorf/Deutsche Krebshilfe and the Medical Faculty of the Heinrich-Heine-University Düsseldorf), the Japan Society for the Promotion of Science (JSPS) KAKENHI Grants-in-Aid for Scientific Research on Innovative Areas (Grant Number 25111005) (to N.M.), and the JSPS Postdoctoral Fellowship (short-term) for North American and European Researchers (Grant Number PE 14784) (to N.H.).

Supplemental Material

Supplemental data for this article can be accessed on the publisher's website.

References

1. Klionsky DJ, Eskelinen EL, Deretic V. Autophagosomes, phagosomes, autolysosomes, phagolysosomes, autophagolysosomes. . . Wait, I'm confused. Autophagy 2014; 10:549-51; PMID:2465794; http://dx.doi.org/10.4161/auto.28448
2. Mizushima N, Yoshimori T, Ohsumi Y. The role of Atg proteins in autophagosome formation. Annu Rev Cell Dev Biol 2011; 27:107-32; PMID:21801009; http://dx.doi.org/10.1146/annurev-cellbio-092910-154005
3. Ganley IG, Lam du H, Wang J, Ding X, Chen S, Jiang X. ULK1.ATG13.FIP200 complex mediates mTOR signaling and is essential for autophagy. J Biol Chem 2009; 284:12297-305; PMID:19258318
4. Hosokawa N, Hara T, Kaizuka T, Kishi C, Takamura A, Miura Y, Iemura S, Natsume T, Takehana K, Yamada N, et al. Nutrient-dependent mTORC1 association with the ULK1-Atg13-FIP200 complex required for autophagy. Mol Biol Cell 2009; 20:1981-91; PMID:19211835; http://dx.doi.org/10.1091/mbc.E08-12-1248
5. Hosokawa N, Sasaki T, Iemura S, Natsume T, Hara T, Mizushima N. Atg101, a novel mammalian autophagy protein interacting with Atg13. Autophagy 2009; 5:973-9; PMID:19597335; http://dx.doi.org/10.4161/auto.5.7.9296
6. Chan EY, Longatti A, McKnight NC, Tooze SA. Kinase-inactivated ULK proteins inhibit autophagy via their conserved C-terminal domains using an Atg13-independent mechanism. Mol Cell Biol 2009; 29:157-71; PMID:18936157; http://dx.doi.org/10.1128/MCB.01082-08
7. Jung CH, Jun CB, Ro SH, Kim YM, Otto NM, Cao J, Kundu M, Kim DH. ULK-Atg13-FIP200 complexes mediate mTOR signaling to the autophagy machinery. Mol Biol Cell 2009; 20:1992-2003; PMID:19225151 http://dx.doi.org/10.1091/mbc.E08-12-1249
8. Mercer CA, Kaliappan A, Dennis PB. A novel, human Atg13 binding protein, Atg101, interacts with ULK1 and is essential for macroautophagy. Autophagy 2009; 5:649-62; PMID:19287211; http://dx.doi.org/10.4161/auto.5.5.8249
9. Alers S, Löffler AS, Paasch F, Dieterle AM, Keppeler H, Lauber K, Campbell DG, Fehrenbacher B, Schaller M, Wesselborg S, et al. Atg13 and FIP200 act independently of Ulk1 and Ulk2 in autophagy induction. Autophagy 2011; 7:1423-33; PMID:22024743; http://dx.doi.org/10.4161/auto.7.12.18027
10. Bach M, Larance M, James DE, Ramm G. The serine/threonine kinase ULK1 is a target of multiple phosphorylation events. Biochem J 2011; 440:283-91; PMID:21819378; http://dx.doi.org/10.1042/BJ20101894
11. Egan DF, Shackelford DB, Mihaylova MM, Gelino S, Kohnz RA, Mair W, Vasquez DS, Joshi A, Gwinn DM, Taylor R, et al. Phosphorylation of ULK1 (hATG1) by AMP-activated protein kinase connects energy sensing to mitophagy. Science 2011; 331:456-61; PMID:21205641; http://dx.doi.org/10.1126/science.1196371
12. Kim J, Kundu M, Viollet B, Guan KL. AMPK and mTOR regulate autophagy through direct phosphorylation of Ulk1. Nat Cell Biol 2011; 13:132-41; PMID:21258367; http://dx.doi.org/10.1038/ncb2152
13. Mack HI, Zheng B, Asara JM, Thomas SM. AMPK-dependent phosphorylation of ULK1 regulates ATG9 localization. Autophagy 2012; 8:1197-214; PMID:22932492; http://dx.doi.org/10.4161/auto.20586
14. Shang L, Chen S, Du F, Li S, Zhao L, Wang X. Nutrient starvation elicits an acute autophagic response mediated by Ulk1 dephosphorylation and its subsequent dissociation from AMPK. Proc Natl Acad Sci USA 2011; 108:4788-93; ; PMID:21383122; http://dx.doi.org/10.1073/pnas.1100844108
15. Lin SY, Li TY, Liu Q, Zhang C, Li X, Chen Y, Zhang SM, Lian G, Ruan K, Wang Z, et al. GSK3-TIP60-ULK1 signaling pathway links growth factor deprivation to autophagy. Science 2012; 336:477-81; PMID:22539723; http://dx.doi.org/10.1126/science.1217032
16. Nazio F, Strappazzon F, Antonioli M, Bielli P, Cianfanelli V, Bordi M, Gretzmeier C, Dengjel J, Piacentini M, Fimia GM, et al. mTOR inhibits autophagy by controlling ULK1 ubiquitylation, self-association and function through AMBRA1 and TRAF6. Nat Cell Biol 2013; 15:406-16; PMID:23524951; http://dx.doi.org/10.1038/ncb2708
17. Di Bartolomeo S, Corazzari M, Nazio F, Oliverio S, Lisi G, Antonioli M, Pagliarini V, Matteoni S, Fuoco C, Giunta L, et al. The dynamic interaction of AMBRA1 with the dynein motor complex regulates mammalian autophagy. J Cell Biol 2010; 191:155-68; PMID:20921139; http://dx.doi.org/10.1083/jcb.201002100
18. Russell RC, Tian Y, Yuan H, Park HW, Chang YY, Kim J, Kim H, Neufeld TP, Dillin A, Guan KL. ULK1 induces autophagy by phosphorylating Beclin-1 and activating VPS34 lipid kinase. Nat Cell Biol 2013; 15:741-50; PMID:23685627; http://dx.doi.org/10.1038/ncb2757
19. Tang HW, Wang YB, Wang SL, Wu MH, Lin SY, Chen GC. Atg1-mediated myosin II activation regulates autophagosome formation during starvation-induced autophagy. EMBO J 2011; 30:636-51; PMID:21169990; http://dx.doi.org/10.1038/emboj.2010.338
20. Cheong H, Lindsten T, Wu J, Lu C, Thompson CB. Ammonia-induced autophagy is independent of ULK1/ULK2 kinases. Proc Natl Acad Sci USA 2011; 108:11121-6; PMID:21690395; http://dx.doi.org/10.1073/pnas.1107969108
21. Chang YY, Neufeld TP. An Atg1/Atg13 complex with multiple roles in TOR-mediated autophagy regulation. Mol Biol Cell 2009; 20:2004-14; PMID:19225150; http://dx.doi.org/10.1091/mbc.E08-12-1250
22. Hara T, Takamura A, Kishi C, Iemura S, Natsume T, Guan JL, Mizushima N. FIP200, a ULK-interacting protein, is required for autophagosome formation in mammalian cells. J Cell Biol 2008; 181:497-510; PMID:18443221; http://dx.doi.org/10.1083/jcb.200712064
23. Fujioka Y, Suzuki SW, Yamamoto H, Kondo-Kakuta C, Kimura Y, Hirano H, Akada R, Inagaki F, Ohsumi Y, Noda NN. Structural basis of starvation-induced assembly of the autophagy initiation complex. Nat Struct Mol Biol 2014 21(6):513-21; PMID:24793651
24. Klionsky DJ, Abdalla FC, Abeliovich H, Abraham RT, Acevedo-Arozena A, Adeli K, Agholme L, Agnello M, Agostinis P, Aguirre-Ghiso JA, et al. Guidelines for the use and interpretation of assays for monitoring autophagy. Autophagy 2012; 8:445-544; PMID:22966490; http://dx.doi.org/10.4161/auto.19496
25. Joo JH, Dorsey FC, Joshi A, Hennessy-Walters KM, Rose KL, McCastlain K, Zhang J, Iyengar R, Jung CH, Suen DF, et al. Hsp90-Cdc37 chaperone complex regulates Ulk1- and Atg13-mediated mitophagy. Mol Cell 2011; 43:572-85; PMID:21855797; http://dx.doi.org/10.1016/j.molcel.2011.06.018
26. Kimura S, Noda T, Yoshimori T. Dissection of the autophagosome maturation process by a novel reporter protein, tandem fluorescent-tagged LC3. Autophagy 2007; 3:452-60; PMID:17534139; http://dx.doi.org/10.4161/auto.4451
27. Nishida Y, Arakawa S, Fujitani K, Yamaguchi H, Mizuta T, Kanaseki T, Komatsu M, Otsu K, Tsujimoto Y, Shimizu S. Discovery of Atg5/Atg7-independent alternative macroautophagy. Nature 2009; 461:654-8; PMID:19794493; http://dx.doi.org/10.1038/nature08455
28. Scarlatti F, Maffei R, Beau I, Codogno P, Ghidoni R. Role of non-canonical Beclin 1-independent autophagy in cell death induced by resveratrol in human breast cancer cells. Cell Death Differ 2008; 15:1318-29; PMID:18421301; http://dx.doi.org//10.1038/cdd.2008.51
29. McAlpine F, Williamson LE, Tooze SA, Chan EY. Regulation of nutrient-sensitive autophagy by uncoordinated 51-like kinases 1 and 2. Autophagy 2013; 9:361-73; PMID:23291478; http://dx.doi.org/10.4161/auto.23066
30. Harris BZ, Lim WA. Mechanism and role of PDZ domains in signaling complex assembly. J Cell Sci 2001; 114:3219-31; PMID:11591811
31. Lee HJ, Zheng JJ. PDZ domains and their binding partners: structure, specificity, and modification. Cell Commun Signal 2010; 8:8; PMID:20509869; http://dx.doi.org/10.1186/1478-811X-8-8
32. Nourry C, Grant SG, Borg JP. PDZ domain proteins: plug and play!. Sci STKE 2003; 2003:RE7; PMID:12709532
33. Chan EY, Kir S, Tooze SA. siRNA screening of the kinome identifies ULK1 as a multidomain modulator of autophagy. J Biol Chem 2007; 282:25464-74; PMID:17595159; http://dx.doi.org/10.1074/jbc.M703663200
34. Tomoda T, Kim JH, Zhan C, Hatten ME. Role of Unc51.1 and its binding partners in CNS axon outgrowth. Genes Dev 2004; 18:541-58; PMID:15014045; http://dx.doi.org/10.1101/gad.1151204
35. Songyang Z, Fanning AS, Fu C, Xu J, Marfatia SM, Chishti AH, Crompton A, Chan AC, Anderson JM, Cantley LC. Recognition of unique carboxyl-terminal motifs by distinct PDZ domains. Science 1997; 275:73-7; PMID:8974395; http://dx.doi.org/10.1126/science.275.5296.73
36. Stjepanovic G, Davies CW, Stanley RE, Ragusa MJ, Kim DJ, Hurley JH. Assembly and dynamics of the autophagy-initiating Atg1 complex. Proc Natl Acad Sci USA 2014 111(35):12793-8; PMID:25139988
37. Liang Q, Yang P, Tian E, Han J, Zhang H. The C. elegans ATG101 homolog EPG-9 directly interacts with EPG-1/Atg13 and is essential for autophagy. Autophagy 2012; 8:1426-33; PMID:22885670; http://dx.doi.org/10.4161/auto.21163
38. Kraft C, Kijanska M, Kalie E, Siergiejuk E, Lee SS, Semplicio G, Stoffel I, Brezovich A, Verma M, Hansmann I, et al. Binding of the Atg1/ULK1 kinase to the ubiquitin-like protein Atg8 regulates autophagy. EMBO J 2012; 31:3691-703; PMID:22885598; http://dx.doi.org/10.1038/emboj.2012.225
39. Löffler AS, Alers S, Dieterle AM, Keppeler H, Franz-Wachtel M, Kundu M, Campbell DG, Wesselborg S, Alessi DR, Stork B. Ulk1-mediated phosphorylation of AMPK constitutes a negative regulatory feedback loop. Autophagy 2011; 7:696-706; PMID:21460634; http://dx.doi.org/10.4161/auto.7.7.15451